RSC Advances

PAPER

View Article Online
View Journal | View Issue

Cite this: *RSC Adv.*, 2016, **6**, 22285

High visible-light photochemical activity of titania decorated on single-wall carbon nanotube aerogels†

Hang-Ah Park, Siyuan Liu, Paul A. Salvador, Gregory S. Rohrer and Mohammad F. Islam*

Photocatalysts are being extensively investigated to convert renewable solar energy into chemical energy but suffer from high costs or low efficiencies. We report on the development of highly visible-light photoactive composites of titania (TiO_2) and single-wall carbon nanotubes (SWCNTs) that rapidly photodegrade methylene blue dyes under visible-light illumination in the absence of cocatalysts. We fabricated these freestanding porous composites of density ≈36 mg mL^{-1} (volume fraction ≈ 0.01) by an *in situ* sol–gel synthesis of titania nanoparticles of diameter ≈9 nm within SWCNT aerogels. The SWCNT aerogels are three-dimensional porous networks of individualized SWCNTs having a density ≈9 mg mL^{-1} (volume fraction ≈ 0.006), whose large surface area and high porosity enable substantial titania loading and unimpeded dye transport to titania. The TiO_2/SWCNT aerogel composites had a surface area of 293 m^2 g^{-1} and pores of diameters between 2–25 nm. X-ray photoelectron spectroscopy showed a strong bonding interaction between titania and SWCNTs (*i.e.*, titanium–carbon and titanium–oxygen–carbon bonds), which possibly rendered these aerogel composites photoactive in visible-light with an absorption edge ≈2.6 eV. In contrast, titania is only active in ultraviolet-light due to its large bandgap (≈3.2 eV). Further, they degraded dyes at a rate of ≈25 μmol g^{-1} h^{-1} with a rate constant of ≈0.012 min^{-1} under visible-light irradiation, values that are more than two times greater than those from other titania-based photocatalysts under visible or ultraviolet illumination. In comparison, titania nanoparticles alone were essentially inactive under similar test conditions. Interestingly, the rate constant for dye degradation decreased with an increase in dye concentration, but the overall rate of degradation remained nearly unchanged. Moreover, the addition of platinum cocatalysts did not improve the photocatalytic performance of the TiO_2/SWCNT composites. These observations suggest that the composites efficiently separate visible-light generated electron–hole pairs and that photodegradation was limited by the availability of reactive sites on titania (the anodic reaction). We postulate that further enhancements are plausible through composite design and that our facile fabrication method can be readily adapted to create nearly any freestanding photocatalyst/SWCNT aerogel composites for use in high performance photoelectrochemical cells.

Received 10th February 2016
Accepted 17th February 2016

DOI: 10.1039/c6ra03801h

www.rsc.org/advances

Introduction

Solar energy, a major renewable energy source, is increasingly being explored to produce hydrogen fuel *via* water splitting,[1–6] to generate electricity in solar cells,[7–9] and to remediate water of heavy metals and organic matter,[10–12] among many other applications through the use of photocatalysts. Titania (TiO_2) is perhaps the most extensively studied photocatalyst because it is abundant, inexpensive, stable in photochemical environments,[13] and generates electron–hole pairs at energy levels appropriate to split water.[14] Unfortunately, titania is a relatively poor photocatalyst because its large bandgap of 3.2 eV only allows titania to absorb ultraviolet (UV)-light, which is only 5% of the total solar energy, and its fast electron–hole recombination rate leads to high losses.[11,15,16] Indeed, titania requires cathodic cocatalysts such as platinum[11] to reduce electron–hole recombination and to generate measurable photoactivity.[11] To overcome these limitations, composites of titania and various carbon materials, such as carbon nanotubes (CNTs),[17–19] graphene,[20–22] and graphite,[23,24] have been explored to narrow titania's bandgap by carbon doping and to reduce photogenerated

Department of Materials Science and Engineering, Carnegie Mellon University, 5000 Forbes Avenue, Pittsburgh, PA 15213, USA. E-mail: mohammad@cmu.edu

† Electronic supplementary information (ESI) available: Comparison table of photocatalytic dye degradation, SEM and TEM images, surface area and pore characteristics, schematic illustration of photocatalytic dye degradation, and equilibrium time for dye adsorption of TiO_2/SWCNT aerogels. See DOI: 10.1039/c6ra03801h

electron–hole recombination through efficient charge transfer from titania to carbon materials.[11,25]

Single-wall CNTs (SWCNTs) are considered ideal supports for photocatalysts because SWCNTs have a large electron storage capability of one electron per 32 carbon atoms that reduces electron–hole recombination,[26–28] have a high specific surface area (SSA) of 1315 $m^2\ g^{-1}$ for photocatalyst loading,[29] can act as a photosensitizer that enlarges titania absorption bandwidth,[30,31] and are highly electrically conducting for efficient charge collection.[26,32] Multiwall CNTs (MWCNTs) have been the most explored CNT-based support for photocatalysts,[17,20,33–35] even though MWCNTs have a much lower SSA of $\approx$150 $m^2\ g^{-1}$ and inferior physical properties to support photocatalysts than SWCNTs;[29] this is likely because SWCNTs are difficult to handle and typically exist as bundles with rather small effective SSA ($\approx$100 $m^2\ g^{-1}$). Both TiO_2/MWCNT and TiO_2/SWCNT composites have demonstrated substantially improved photocatalytic activity when compared to titania alone, typically evaluated by measuring degradation of dyes such as methylene blue or rhodamine B. For example, commercially available titania particulates (P25) deposited on MWCNTs or titania synthesized on MWCNTs *in situ* have both been shown to form Ti–O–C (titanium–oxygen–carbon) or Ti–C bonds with MWCNTs, resulting in an enlargement in the absorption bandwidth compared to titania and leading to significantly enhanced dye degradation rates of $\approx$15 $\mu mol\ g^{-1}\ h^{-1}$ under visible-light irradiation compared with negligible capability of titania alone.[20,36] Similarly, TiO_2/SWCNT composites exhibit $\approx$2 times greater dye degradation rates ($\approx$11 $\mu mol\ g^{-1}\ h^{-1}$) compared with titania alone ($\approx$5 $\mu mol\ g^{-1}\ h^{-1}$) under UV-light.[21] A comparison of relevant studies involving titania on CNTs is presented in Table 1. Further improvements are likely if titania could be incorporated on high SSA SWCNTs and/or SWCNT networks that have high carrier transport capability.

In this work, we report on the development of aerogel composites of titania and SWCNTs that are photoactive in the visible-light region. The composites were fabricated by synthesizing *in situ* titania nanoparticles on SWCNTs aerogels. These SWCNT aerogels are freestanding three-dimensional (3D) networks of mostly individual nanotubes[37] that have ultrahigh surface area, which allows for substantial deposition of titania, and >99% porosity, which allows unimpeded transport of dyes to titania. We used high-resolution electron microscopy imaging, specific surface area analysis, and Raman and X-ray photoelectron spectroscopy to characterize the microstructure and bonding in these TiO_2/SWCNT aerogels. Finally, the photocatalytic performance of TiO_2/SWCNT aerogel composites was investigated by measuring the degradation rates and rate constants of methylene blue dye under visible-light irradiation. The results demonstrate that significant improvements in photocatalytic activity are achieved for TiO_2/SWCNT composites.

Results and discussion

The major steps in the synthesis of TiO_2/SWCNT aerogels are schematically illustrated in Fig. 1. A photograph of freestanding SWCNT and TiO_2/SWCNT aerogels is given in Fig. 2a. The SWCNT aerogels appeared black, whereas the TiO_2/SWCNT aerogels were slightly grey due to titania. High-resolution scanning electron microscope (SEM) and conventional-resolution transmission electron microscope (TEM) images of cross-sections of TiO_2/SWCNT aerogels are given in Fig. 2b and c, respectively. These show that the porous, uniform, and isotropic nanotube network of the underlying SWCNT aerogels remained intact through the titania deposition process (similar images of cross-sections of SWCNT aerogels are given in Fig. S1†). Interestingly, titania nanoparticles were often located at the nodes between SWCNTs, likely because titania nanoparticles preferentially nucleated at the nodes, which have a lower surface energy compared to the struts. The average diameter of the titania nanoparticles was $\approx$9 nm. Based on the total titania mass in the TiO_2/SWCNT aerogels and the average titania nanoparticle diameter measured here, we estimate the

Table 1 Comparison of photocatalytic dye degradation performance by TiO_2 supported on CNTs

Photocatalysts	Light source, power, spectral range	Adsorption–desorption equilibration time [h]	Dye : titania molar ratio[a]	Degradation rate[a] [$\mu mol\ g^{-1}\ h^{-1}$]	Rate constant[a] [min^{-1}]	Ref.
TiO_2/SWCNT aerogels	Hg, 300 W, visible	24	0.004	25 200[b]	0.012	This work
		24	0.032	25 (with fresh 0.02 mM dye solution)	0.0015	
TiO_2 P25/MWCNT	Xe, 500 W, visible	0.167	0.002	15	0.011	20
TiO_2/MWCNT	Xe, 450 W, visible	1	0.024	13[c]	0.007	33
TiO_2/inside of MWCNT	Xe, visible	2	0.012	98[c]	0.058	34
TiO_2/N-doped MWCNT	Xe, 450 W, visible	1	N.A.[d]	N.A.[d]	0.014	17
TiO_2/SWCNT	20 W, UV	1	0.005[e]	11	0.19	36
TiO_2/MWCNT	125 W, UV	0.5	0.006[f]	102[c]	0.080	35

[a] After dye adsorption to the samples had reached equilibrium in the dark. [b] Estimated by taking the starting concentration of dyes before adsorption–desorption equilibration as C_0. [c] Estimated by taking the starting concentration of dyes before adsorption–desorption equilibration as C_0 because the dye concentrations after equilibration are not provided. As such, the degradation rates and rate constants are likely to be significantly overestimated, particularly if supports had large surface area for dye adsorption. [d] Used thin film of dimensions 0.8 cm × 0.8 cm. Sample masses were not reported. [e] Used rhodamine B dye. [f] Used reactive orange 16 dye.

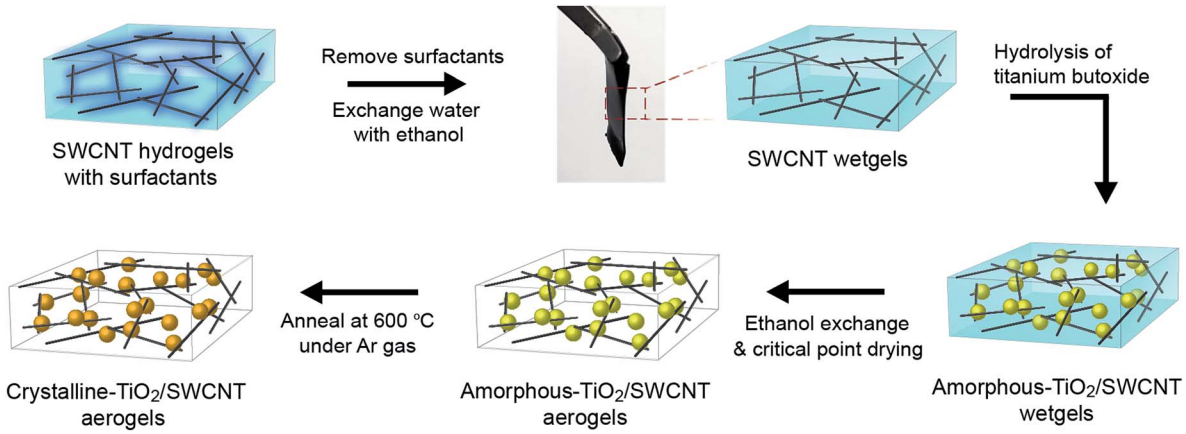

Fig. 1 Schematic illustration of the synthesis process for TiO_2/SWCNT aerogels.

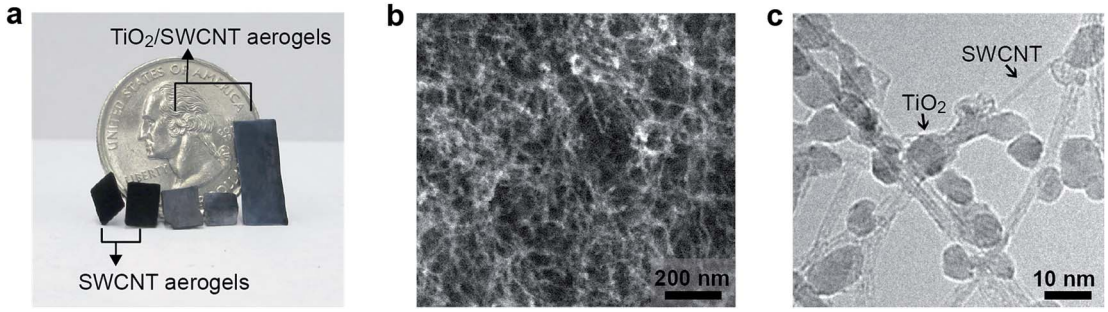

Fig. 2 (a) A photograph of freestanding SWCNT and TiO_2/SWCNT aerogels. (b) A high-resolution SEM and (c) a conventional-resolution TEM image of cross-sections of TiO_2/SWCNT aerogels.

titania nanoparticle loading per unit cross-sectional area to be $\approx 1.25 \times 10^{18}$ nanoparticles cm^{-2}.

We further characterized the microstructure of TiO_2/SWCNT aerogels by measuring the SSA and the pore size distributions using Brunauer–Emmet–Teller (BET) and Barrett–Joyner–Halenda (BJH) methods. The BET surface area of the underlying SWCNT aerogels of density 9 mg mL^{-1} was 857 m^2 g^{-1}, which decreased to 293 m^2 g^{-1} after 27.5 mg mL^{-1} of titania loading; the BET based SSA for both type of aerogels were calculated from the measured adsorption data shown in Fig. S2a.† This value is still significantly larger than that reported for other TiO_2/CNT composites.[17,33,35,36] The BJH pore sizes of the TiO_2/SWCNT aerogels were between 2 and 25 nm, with a majority of pores being less than 10 nm. In contrast to SWCNT aerogels, TiO_2/SWCNT aerogels had a substantially smaller fraction of pores with diameters less than 5 nm, likely because those pores became closed by titania nanoparticles (Fig. S2b†). Nevertheless, the pores are large enough to allow for facile transport of dye and ionic species. Note that both titania and SWCNT surfaces can adsorb dye molecules (the latter *via* π–π interactions on the SWCNT)[20] and facilitate dye degradation during light irradiation.

The crystallinity and the relevant phases of titania in the TiO_2/SWCNT aerogels were determined using powder X-ray diffraction (XRD) and a representative XRD pattern is shown in Fig. 3a. The pattern displayed distinct diffraction peaks associated with both the anatase (JCPDS 21-1272) and the rutile (JCPDS 04-0551) crystalline phases, and are identified by "A" and "R", respectively, in Fig. 3a. The annealing of TiO_2/SWCNT aerogels at 600 °C that typically transforms titania from anatase phase to rutile phase likely caused titania in our samples to possess both types of phases.

The structural integrity of the TiO_2/SWCNT composites and the interactions between titania and the SWCNTs were characterized using Raman spectroscopy (Fig. 3b and c), and compared with titania and SWCNTs. The Raman spectra from TiO_2/SWCNT aerogels displayed distinct features associated with SWCNTs as well as anatase (A) and rutile (R) titania (Fig. 3b). The intensity ratio I_D/I_G between the SWCNT D-band at ≈ 1300 cm^{-1}, which characterizes the sp^3-hybridized carbon in the aerogels,[38] and the G-band at ≈ 1591 cm^{-1} of TiO_2/SWCNT aerogels relative to pristine SWCNT aerogels was used to characterize damage or structural defects in SWCNTs from titania deposition. Note that the G-band is a characteristic Raman feature of SWCNTs and quantifies the sp^2-hybridized carbon bonds in the aerogels. The I_D/I_G for TiO_2/SWCNT aerogels increased only slightly to 0.11 from 0.07 for SWCNT aerogels, indicating only minimal damage to SWCNTs from titania deposition. Moreover, the Raman spectra displayed radial breathing modes (RBMs), which are exclusive features of

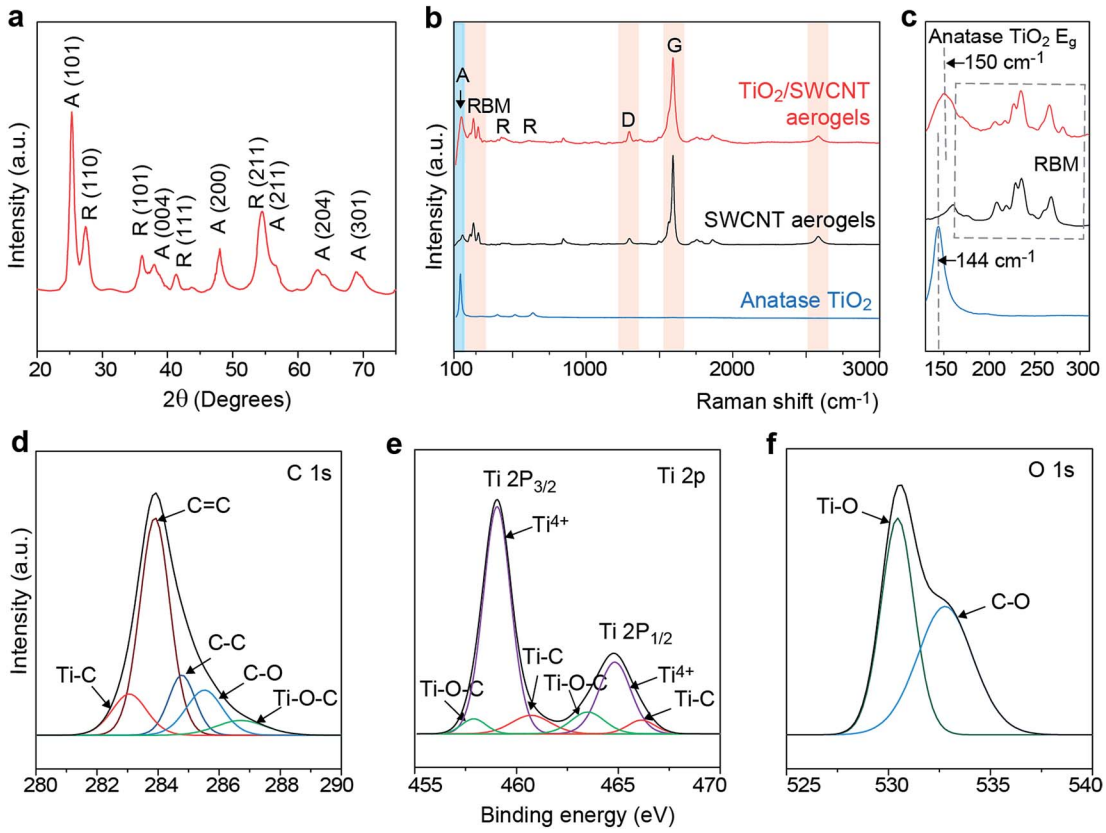

Fig. 3 (a) X-ray diffraction pattern of TiO_2/SWCNT aerogels. (b) Raman spectra from TiO_2/SWCNT aerogels, SWCNT aerogels, and anatase titania. (c) The anatase E_g and RBM modes of titania and SWCNTs, respectively. X-ray photoelectron spectroscopy (XPS) spectra from TiO_2/SWCNT aerogels for (c) 1s core level of carbon (C), (d) 2p core level of titanium (Ti), and (e) 1s core level of oxygen (O), suggesting Ti–C and Ti–O–C bonding between TiO_2 and SWCNTs.

SWCNTs, establishing that the SWCNTs remained intact in these TiO_2/SWCNT aerogels. Finally, the Raman spectra from pure anatase titania and TiO_2/SWCNT aerogels were compared. The in-house synthesized anatase titania powder was made using the same chemical reagents with identical reagent concentrations and reaction conditions that were used to synthesize TiO_2 within SWCNT aerogels, but the titania powder was annealed at 450 °C in air. The characteristic E_g mode associated with anatase titania was blue shifted by 6 cm^{-1} from 144 cm^{-1} for pure anatase titania to 150 cm^{-1} for TiO_2/SWCNT aerogels, indicating strong interactions between titania and SWCNTs, likely at the interface between the nanoparticles and SWCNTs. In spite of these strong interactions, there is only a minimal impact on the SWCNT structure. The intensities of Raman peaks at 439 cm^{-1} and 608 cm^{-1} in the spectra from TiO_2/SWCNT aerogels, which we attribute to rutile titania,[39] were very small. Hence, we did not compare any shifts to these peaks to Raman peak from pure rutile titania.

The interactions between titania and SWCNTs were further investigated using X-ray photoelectron spectroscopy (XPS), focused on the C 1s, Ti 2p, and O 1s spectra (given respectively in Fig. 3c–e). The 1s core level spectrum of C can be deconvolved into five peaks (Fig. 3c). The two dominant peaks arise from SWCNTs, being the C=C peak at 283.8 eV and the C–C peak at 284.9 eV. The third largest peak arises from the C–O peak at 285.8 eV, which suggests that some oxygen formed bonds with SWCNTs. The last two peaks are associated with Ti and C interactions: a Ti–C peak at 282.4 eV and Ti–O–C peak at 287.2 eV. These last two peaks imply that bonding occurs between titania and carbon. Signatures of these bonds were also present in the deconvolved 2p core level spectrum of Ti (Fig. 3d). The Ti–O (Ti^{4+}) $2p_{3/2}$ and $2p_{1/2}$ peaks observed respectively at 459 eV and 464.8 eV are the primary peaks. In addition, Ti–C peaks are observed at 460.6 and 466.0 eV, and Ti–O–C peaks are observed at 457 and 463 eV. Finally, the 1s core level spectrum of O (Fig. 3e) can be fitted into two peaks. The first peak at 530.5 eV can be attributed to Ti–O, while the peak at 532.7 eV can be attributed to C–O. Overall, XPS results support a strong bonding interaction between titania and SWCNTs within TiO_2/SWCNT aerogels, which could explain the small increase in I_D/I_G in Raman spectra for TiO_2/SWCNT aerogels (Fig. 3b). The structural integrity of SWCNTs, illustrated by Raman data, and the strong interactions between titania and SWCNTs should facilitate fast electron transfer into nanotubes, leading to a reduction in recombination of photogenerated electron–hole pairs and an enhancement in photocatalytic efficiency of the TiO_2/SWCNT aerogels.

The optical absorbance properties of the TiO_2/SWCNT aerogels and related materials, measured using UV-visible (vis)

reflectance spectroscopy, are shown in Fig. 4. Anatase titania showed a significant reflectance across the visible spectrum, whereas the SWCNT and TiO_2/SWCNT aerogels showed minimal reflectance over the same range. To estimate the absorption edge of the TiO_2/SWCNT aerogel composites, we calculated the Kubelka–Munk function, $F(R)$, from the reflectance (R) using the expression $F(R) = (1 - R)^2/2R$ and then plotted $[F(R)h\nu]^{1/2}$ as a function of photon energy $h\nu$.[40,41] This type of plot is commonly known as a Tauc plot and is widely used to estimate bandgaps of materials.[42,43] Using this method, the anatase titania bandgap was observed near the expected value of ≈3.2 eV.[44] The SWCNT aerogels did not show a characteristic absorption edge, but rather a broad absorbance in the visible spectrum. The TiO_2/SWCNT aerogels showed intermediate behavior, exhibiting a baseline broad absorbance in the visible spectrum (attributed to the SWCNTs) with an abrupt increase near ≈2.6 eV reminiscent of the anatase band edge absorption. In spite of the qualitative similarity, the absorption edge related to the anatase is shifted significantly into the visible region compared to pure anatase, likely because of the interfacial bonding between titania and carbon that was revealed through the Raman and XPS data.

The titania deposition within SWCNT aerogels substantially improved the mechanical integrity of the nanotube networks in an aqueous environment. This is illustrated by the stability of the sample volume with respect to time in water (shown in Fig. 5). The SWCNTs within the aerogels are held together only *via* van der Waals interactions at the nodes between the nanotubes.[45,46] As a result, SWCNT aerogels undergo structural collapse or significant plastic deformation (of >80%) in volume (as shown in Fig. 5a) when they are submerged into water (or many other fluids), due to capillary forces arising from fluids wicking into the nanopores. Surprisingly, the volume of TiO_2/SWCNT aerogels only decreased by ≈15% when they submerged into water. This can be rationalized if titania nanoparticles at nodes (see Fig. 2c) hinder nanotube rotation around the nodes, which is required for the aerogel to collapse.[46,47] A schematic of possible deformation pathways for

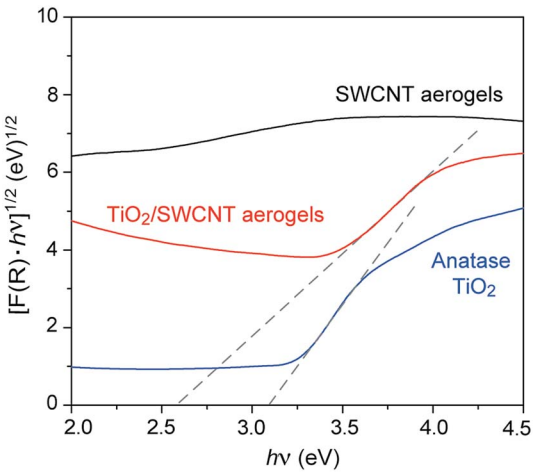

Fig. 4 Tauc plot of $[F(R)h\nu]^{1/2}$ *versus* photon energy, $h\nu$, to estimate absorption edge of TiO_2/SWCNT aerogels.

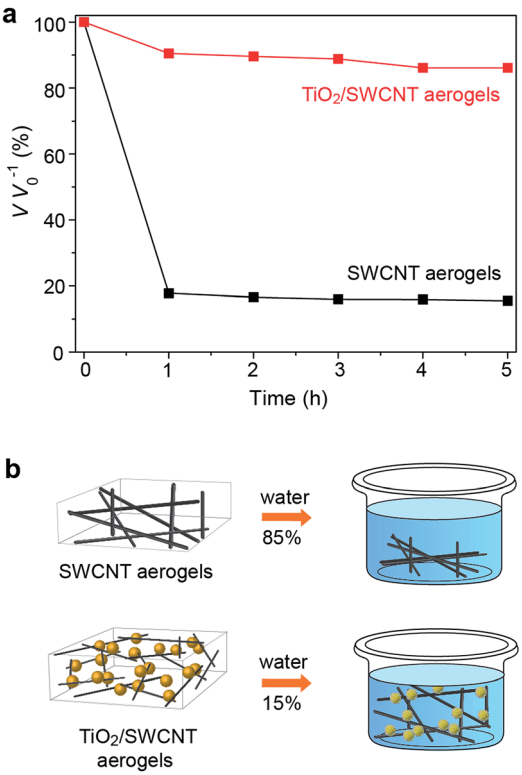

Fig. 5 Titania enhances the structural stability of the underlying SWCNT aerogels. (a) Decrease in aerogel volumes after submersion in water for 5 h. V_0 is the initial volume of aerogels and V is the volume after submersion into water. (b) Schematic illustration of the possible deformation processes of aerogels in water.

SWCNT and TiO_2/SWCNT aerogels in water is given in Fig. 5b. Importantly, this improved stability allowed the aerogel composites to be tested for their photocatalytic performance as freestanding structures. Furthermore, it may also make it possible to use them as stable electrodes (anodes) in photoelectrochemical cells. However, the bonding between titania and SWCNTs along with infiltration of the nodes between SWCNTs by titania, which improve visible-light absorption and mechanical stability, significantly reduced the electrical conductivity of the underlying SWCNT aerogels. The native SWCNT aerogels had a conductivity of ≈1.5 S cm^{-1},[47] while the TiO_2/SWCNT aerogels had a conductivity of 0.08 S cm^{-1} (the conductivity of anatase titania was ≈10^{-12} S cm^{-1}).[48] This decrease is likely related to the bonding between titania and SWCNTs, which is expected to disrupt the continuous sp^2-hybridized carbon bonds in the SWCNTs, and infiltration of the nodes by insulating titania that affected contacts between SWCNTs.

The photocatalytic activity of TiO_2/SWCNT aerogels was determined by measuring dye degradation over time under visible-light irradiation, and was compared to similar measurements on the dye alone, titania P25 particulates, and SWCNT aerogels. The dye concentration remained constant between 18–24 h for TiO_2/SWCNT aerogels submerged in dye solution in the dark (as shown in Fig. S4†), confirming that the

dye adsorption on the aerogels reached equilibrium. The dye degradation for all samples is shown in Fig. 6, in which $\ln(C\ C_0^{-1})$ is plotted *versus* time (keeping in mind that C_0 is the dye concentration after adsorption equilibration). Samples containing dye alone and titania P25 degraded negligible amounts of dye, and SWCNT aerogels degraded only slightly more. In contrast, TiO_2/SWCNT aerogels were much more active for dye degradation. To determine the dye degradation rate constant, k, it is customary to fit a pseudo-first-order model expressed as:[12,49,50] $\ln(C\ C_0^{-1}) = -kt$, where C is the concentration of dye after a light exposure time, t. Using this model, k values of $\approx 1 \times 10^{-4}$, 1×10^{-4}, and 5×10^{-4} min^{-1} were measured respectively for the dye alone, the titania P25 particulates, and the pristine SWCNT aerogels. The TiO_2/SWCNT aerogels had a rate constant that was more than two orders of magnitude larger at $\approx 120 \times 10^{-4}$ min^{-1}. The degradation rate constant depends on the dye concentration and the molar ratio between the dye and the photocatalyst. Consequently, the photocatalytic dye degradation was assessed by the amount decomposed by unit mass of photocatalyst per unit time: *i.e.*, in units of μmol g^{-1} h^{-1}. In this method, the degradation rates for titania alone and pristine SWCNT aerogels were 0.1 μmol g^{-1} h^{-1} and 5 μmol g^{-1} h^{-1} (per SWCNT mass), respectively; note that no degradation rate for dye alone was calculated since the test sample did not have any photocatalyst. The degradation rate for the TiO_2/SWCNT aerogels was 25 μmol g^{-1} h^{-1}, which is approximately two times larger than reported for any other comparable TiO_2/CNT composites. Also note that taking C_0 to be the initial dye concentration (*i.e.*, 0.02 mM) leads to significant overestimation of the degradation rate (≈200 μmol g^{-1} h^{-1}). A comparison of our results with relevant titania and CNT based composites are presented in Table 1, which includes experimental conditions, rate performance, and other characteristics (similar comparisons for titania supported on carbon, graphene and graphite are given in Table S1†). The TiO_2/SWCNT aerogels maintained their mechanical integrity throughout the dye degradation experiments. Further, Raman spectroscopy showed that SWCNTs did not develop additional defects during these experiments. We also note that the transparency of SWCNT aerogels of thicknesses greater than ≈100 μm is nearly zero.[51] Consequently, titania deposited within SWCNT aerogels beyond this thickness would make negligible contribution to photocatalytic dye degradation, and a thinner TiO_2/SWCNT aerogel should provide a significantly larger dye degradation rate. Furthermore, while the very high porosity of the SWCNT aerogels leads to a relatively high volume for the amount of catalyst that contributed to large dye degradation rates, tuning of titania : SWCNT mass ratio may provide additional enhancement to dye degradation, which we plan to explore in the future.

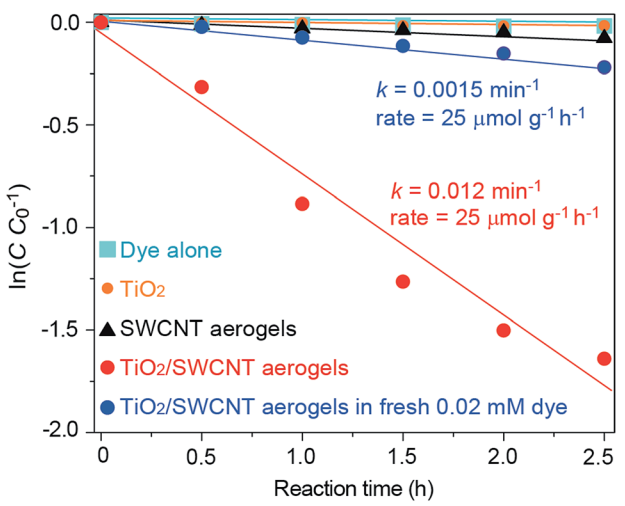

Fig. 6 Photocatalytic methylene blue dye degradation for samples containing dye alone, titania P25 particulates, SWCNT aerogels, and TiO_2/SWCNT aerogels, TiO_2/SWCNT aerogels in fresh 0.02 mM dye solution under visible-light irradiation (λ > 420 nm) after adsorption–desorption equilibration in the dark for 24 h.

To assess the dependence of the dye degradation on C_0, a subset of TiO_2/SWCNT aerogels were transferred to a fresh dye solution of concentration 0.02 mM after being soaked in 0.02 mM dye solution for 24 h in the dark. Notice that C_0 for this set of experiments (≈0.02 mM) was an order of magnitude larger than C_0 in the previous set of experiments in which the equilibrated samples were kept in the dye solution containing residual unadsorbed dye (≈0.0025 mM). The dye degradation results from these samples are shown in Fig. 6. The rate constant was ≈6× smaller ($\approx 15 \times 10^{-4}$ min^{-1}) but the dye degradation rate was identical (25 μmol g^{-1} h^{-1}). This implies that the dye photodegradation capability of the TiO_2/SWCNT aerogel composites was limited by photocatalytic reactive sites and, hence, can be further enhanced using photocatalysts better than titania.

Because the photochemical performance of titania is often improved through the addition of cocatalysts, we characterized the photochemical performance of Pt/TiO_2/SWCNT and TiO_2/Pt/SWCNT aerogels having the same platinum weight loading. The Pt/TiO_2/SWCNT exhibited significantly lower dye degradation rate under visible-light irradiation than the TiO_2/SWCNT aerogels (see Fig. 7), likely because platinum nanoparticles coated titania surfaces and thereby reduced the number of photocatalytically reactive sites. In support of this, the samples in which TiO_2 was deposited after the Pt, or the TiO_2/Pt/SWCNT aerogels, produced similar dye degradation rates to those of TiO_2/SWCNT aerogels under the same light irradiation. These results indicate that the TiO_2/SWCNT aerogel composites are not rate limited by the cathodic reaction, implying that separation and usage of the photogenerated carriers are rapid in these novel nanocomposites. This is supported by the observation that the extremely high rate of photoactivity in these materials is limited by reaction sites at the surface.

Lastly, we evaluated reusability of TiO_2/SWCNT aerogel composites for methylene blue dye degradation. We show the degradation rate constants and degradation rates in Fig. S5.† Note that we kept the experimental conditions, such as dye adsorption–desorption equilibration time, initial dye concentration, and dye : titania molar ratio to be the same. Both k and the degradation rate during the second dye degradation cycle decreased by ≈25%. During third cycle, again k and the degradation rate decreased by another ≈22%. We noticed that

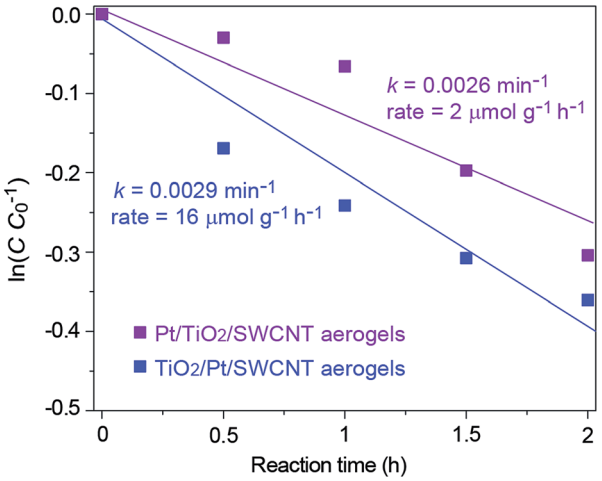

Fig. 7 Photocatalytic degradation of methylene blue by Pt/TiO_2/SWCNT aerogels and TiO_2/Pt/SWCNT aerogels under visible-light irradiation. Photodegradation capability of TiO_2/SWCNT did not improve with addition of Pt, suggesting that SWCNTs alone were sufficient at separating electron–hole pairs generated in TiO_2 under light irradiation.

the amount of dye adsorbed on TiO_2/SWCNT aerogels during the dark equilibration time also decreased by ≈15% in each reuse cycle. We imagine that dyes that adsorbed on SWCNTs but were not photodegraded could not be completely removed by rinsing the composites with water, resulting in lower dye adsorption during equilibration time, k, and degradation rates when the composites were reused. It is also plausible that some of the titania was dislodged from the composites during the rinsing step that we used to remove undegraded dye before reuse.

Experimental

Fabrication of SWCNT hydrogels and wetgels

Fabrication methods for SWCNT hydrogels, wetgels, and aerogels have been reported elsewhere.[45,47,52,53] Briefly, purified SWCNTs (CoMoCAT CG 200; Southwest Nanotechnologies) with diameters of 1.0 ± 0.3 nm and lengths of ≈1 μm were mixed with sodium dodecylbenzene sulfonate surfactant (SDBS; Acros Organics) at a SWCNT concentration of 1 mg mL^{-1} and a SWCNTs : SDBS weight ratio of 1 : 10 in deionized water (Ultrapure Milli-Q, resistivity 18.2 MΩ cm).[45,51,52] The mixtures were sonicated for 2 h at a power of 60 W using a probe tip sonicator (Thermo Fisher 500). The SWCNTs-SDBS suspensions were then centrifuged at 125 000 × g for 19 min (Beckman Coulter Optima™ L-100 K) to pallet bundles and retain mostly isolated nanotubes in the supernatant. The supernatant was decanted and the SWCNT concentration was measured using UV-vis-near infrared (NIR) spectroscopy (Cary 5000; Varian) with a known extinction coefficient of 2.6 (absorbance mL) $(mg\ mm)^{-1}$ at a wavelength of 930 nm.[54] The suspensions were then concentrated to a final nanotube concentration of 3.5 mg mL^{-1} where SWCNTs-SDBS suspensions typically form gels within a few hours.[53,55] We loaded SWCNTs-SDBS suspensions into glass capillaries (Vitrocom) and held them for 12 h to allow the suspensions to form hydrogels;[46,55] the glass capillaries acted as molds to provide suitable shapes to the hydrogels for subsequent experiments. The surfactants were washed-off using 1 M nitric acid for 20 min at 50 °C. The hydrogels were removed from the capillaries and washed thoroughly with deionized water. Since titania could not be deposited on SWCNTs gels in water, we exchanged the water with solutions of increasing concentration of ethanol (EtOH) until the SWCNT networks were in pure anhydrous ethanol; hereinafter such SWCNT networks in ethanol are referred to as SWCNT wetgels. In parallel, pristine SWCNT aerogels were fabricated by removing the anhydrous ethanol through a critical point drying process.[45,47] The SSA, pore structure, and mechanical characteristics of SWCNT aerogels have been reported elsewhere.[47]

Fabrication of TiO_2/SWCNT aerogels

To synthesize titania nanoparticles on SWCNTs *via* the sol–gel method,[40] titanium butoxide (TBOT; Acros Organics) was dissolved in anhydrous ethanol under a nitrogen atmosphere at a TBOT : EtOH molar ratio of 1 : 100. The SWCNT wetgels were soaked in the TBOT solution for 2 h at 50 °C and then were removed from TBOT solution. Excess solution was wiped from the wetgel surfaces using a wet lint-free wiper (Kimwipes; Kimtech) to prevent titania formation on the surfaces. TBOT was hydrolyzed to make titania by adding water dropwise to an amount that was about half the volume of the hydrogels. The hydrolysis process was allowed to proceed for a half an hour, after which the wetgels were washed with ethanol several times to remove unreacted TBOT; note, titania that formed within the wetgels was amorphous. To transform amorphous-TiO_2/SWCNT wetgels into aerogels, the ethanol was thoroughly exchanged with anhydrous ethanol, which was followed by critical point drying (Autosamdri 815, Tousimis) to remove anhydrous ethanol. Finally, we annealed amorphous-TiO_2/SWCNT aerogels at 600 °C for 2 h in argon to crystallize titania.

Fabrication of Pt/TiO_2/SWCNT and TiO_2/Pt/SWCNT aerogels

To investigate the effect of metal cocatalysts on photocatalytic performance, Pt/TiO_2/SWCNT aerogel composites were prepared by depositing platinum nanoparticles within TiO_2/SWCNT aerogels. TiO_2/SWCNT aerogels were soaked in an aqueous solution of 10 mM hexachloroplatinic acid (H_2PtCl_6) under a low vacuum for ≈1 h to remove any air bubbles trapped inside the aerogels and to facilitate solution infiltration. The samples were removed and were gently wiped using a wet lint-free wiper (Kimwipes; Kimtech); this removed excess solution from the surfaces and prevented platinum from forming at the surfaces in the next step. To create platinum nanoparticles, the H_2PtCl_6 solution within the gel was reduced by dropwise addition of 0.5 mL of sodium borohydride ($NaBH_4$) solution, which was prepared by mixing 40 mM $NaBH_4$ with 20 mM of sodium hydroxide (NaOH) solution. The reduction process was allowed to proceed for ≈30 min, after which the sample was washed with deionized water to remove unreacted H_2PtCl_6, $NaBH_4$, and NaOH solutions. Next, the water inside of the Pt/TiO_2/SWCNT

hydrogels was exchanged with solutions of increasing concentration of ethanol until the gels were in pure anhydrous ethanol. These gels were finally dried with a critical point dryer.

TiO_2/Pt/SWCNT aerogels were fabricated by first making SWCNT hydrogels, then depositing platinum nanoparticles onto SWCNTs, followed by exchanging water with anhydrous ethanol, and lastly growing titania within Pt/SWCNT wetgels. The reagents and their concentrations, as well as the synthesis steps for making platinum and titania nanoparticles, were identical to the process described in previous sections.

The dimensions of pristine SWCNT aerogels were 25 mm × 3.5 mm × 0.35 mm (length × width × thickness), which were determined by the glass capillary, and had a mass of 0.28 mg, measured using a balance (XS205; Mettler Toledo) that has a resolution of 0.01 mg, corresponding to an average density ≈9 mg mL^{-1} and an average volume fraction of ≈0.006. The dimensions of the SWCNT aerogels remained the same but the masses increased after decorating with titania and platinum, which we measured using the same balance. The average density of the TiO_2/SWCNT aerogels was ≈36 mg mL^{-1}, which corresponds to a volume fraction of ≈0.01, a titania mass loading per unit cross-sectional area of 2 mg cm^{-2}, and a porosity of ≈99%. The platinum mass loading within the Pt/TiO_2/SWCNT and TiO_2/Pt/SWCNT aerogels was ≈0.35 mg mL^{-1}, while the titania and SWCNT values were similar to those in the TiO_2/SWCNT aerogels.

Microstructure characterization

High-resolution SEM and conventional-resolution TEM images were taken with a spherical aberration corrected FEI Quanta 600 and a Tecnai F20 at 200 kV, respectively. The Raman spectra were collected using a Raman confocal microscope (inVia Raman microscope, Renishaw) with a 50×, 0.75 N.A. air objective (Leica Microsystems) and with a 785 nm (1.58 eV) laser. The laser power was set to 10 mW, the spot size was ≈1–2 μm, and exposure times were ≈1 s. Five scans were collected at every location, and five different locations were investigated for each sample to verify uniformity. The results of the 25 scans were averaged to improve the signal-to-noise ratio. Each Raman spectrum was normalized by its G-band intensity. Data collection and analysis was done with the WiRE software (Renishaw). SSA, pore diameter ($2r$), pore volume (V), and pore diameter distributions (dV/dr) of SWCNT and TiO_2/SWCNT aerogels were determined using nitrogen adsorption and desorption measurements carried out at 77 K in a surface area analyzer (Micromeritics Gemini VII 2390) and calculated with the BET method.[56] The pore diameters, pore volume, and pore diameter distributions were calculated using the BJH method[57] using the desorption branch of the isotherms. XRD was measured using CuKα radiation (λ = 1.54056 Å) with X'Pert Pro MPD X-ray Diffractometer at 40 kV and 30 mA. We collected XPS data with a DESA 150 analyzer (Staib instruments) and AlKα X-rays from a TX400/2 X-ray gun (PSP vacuum technology) as a probe. Elemental analysis was carried out using CasaXPS. The absorbance characteristics of titania and all the aerogels were measured using a Cary 5000 UV-vis-NIR spectrometer (Varian), and their reflectance characteristics were measured using a OL 770-LED multichannel spectroradiometer with a cold cathode mercury (Hg) vapor lamp as a light source.

Structural stability characterization by immersion in water

Both freestanding SWCNT and TiO_2/SWCNT aerogels of known physical dimensions were submerged in distilled water, placed in a low vacuum environment to facilitate water infiltration into the nanopores of the aerogels, and removed from the vacuum once air bubbles stopped escaping from the aerogels (≈15 min). Such samples were then held in water for ≈5 h while their physical dimensions were measured once per hour.

Photocatalytic degradation of methylene blue dye

For dye degradation experiments we cut the aerogels into dimension of 7.5 mm × 3.5 mm × 0.35 mm (length × width × thickness), and calculated mass of each component based on the average densities of the pristine, TiO_2/SWCNT, TiO_2/Pt/SWCNT and Pt/TiO_2/SWCNT aerogels. Test samples were either 0.25 mg of titania P25 particulates, 0.08 mg of SWCNT aerogels, 0.33 mg of TiO_2/SWCNT aerogels (composed of 0.25 mg titania and 0.08 mg SWCNTs), or 0.333 mg of TiO_2/Pt/SWCNT or Pt/TiO_2/SWCNT (composed of 0.25 mg titania, 0.003 mg platinum, and 0.08 mg SWCNTs). To measure photocatalytic performance, a test sample was stirred using a magnetic stir bar in 5 mL of an aqueous solution having 0.02 mM methylene blue in a glass vial for 24 h in the dark to achieve equilibrium for dye adsorption on the test sample prior to visible-light irradiation. To confirm that the dye adsorption on the test sample equilibrated during 24 h of soaking, 0.5 mL of dye solution was periodically removed and its absorbance characterized beginning at 18 h. Note that the aerogels were suspended in solution using a metal mesh to avoid any mechanical disintegration from collision with magnetic stir bar. The dye concentration in solution was dramatically decreased after the 24 h equilibration time; hence, in all photocatalysis experiments, the value of C_0 corresponded to the value measured after the dye adsorption equilibration. For the reusability test, we removed the test sample from the dye solution after the 1st cycle of visible-light dye degradation measurements, rinsed it in water, and then soaked it in a 0.02 mM dye solution in the dark for 24 h to achieve dye adsorption equilibration. Next, we measured the residual dye concentration in the solution to determine dye adsorption on test samples during the 2nd cycle. We submerged the test sample in a dye solution with the same C_0 used in 1st cycle to maintain the same dye : titania molar ratio and measured dye degradation. We repeated this process for the 3rd cycle and again measured the dye degradation. The light source was a 300 W Hg lamp that had: a UV cut-off filter that transmitted light with wavelengths $\lambda > 420$ nm, an IR cut-off filter that blocked light with $\lambda \geq 1200$ nm, and a cooling system. We periodically measured the absorbance of the dye solution using a Varian Cary 5000 UV-vis-NIR spectrometer by sampling 0.5 mL of the solution; note that for mixtures containing titania P25, we first centrifuged the withdrawn solution at 21 000 × g to sediment the P25 particles prior to absorbance measurements. Photocatalytic

dye degradation measurements at each condition were repeated with at least three different samples.

Conclusions

We have developed freestanding TiO_2/SWCNT aerogel composites that have high visible light photoactivity. These composited were made by uniformly decorating aerogels of individually dispersed SWCNTs with titania nanoparticles. The bulk SWCNT aerogels have ultrahigh surface area and are able to support large amounts of titania nanoparticles, to maintain high porosity for efficient dye and ion transport, even after titania loading, and to retain high electrical conductivity for rapid distribution of charge carrier pairs. The results support strong bonding interactions between the titania and the SWCNTs without significant structural damage to nanotubes, which afford strong visible light absorption and facile electron injection into nanotubes that hinders recombination of photogenerated electron–hole pairs. Consequently, these TiO_2/SWCNT aerogels exhibited high photochemical activity as evidenced by their rapid dye degradation capabilities. We postulate that our fabrication approach could be adapted to many other higher performing photocatalysts to create anodes that in turn can enhance the performances of photoelectrochemical fuel cells, solar cells, and energy storage and conversion systems.

Acknowledgements

This work was supported by the National Science Foundation through grant CMMI-1335417 (M. F. I.) and DMR-1206656 (G. S. R. and P. A. S.), and Philip and Marsha Dowd fellowship (H.-A. P). We acknowledge the use of the Carnegie Mellon Materials Characterization Facility at Carnegie Mellon University (supported by grant MCF-677785) for TEM and SEM imaging.

Notes and references

1 P. Hartmann, D. K. Lee, B. M. Smarsly and J. Janek, *ACS Nano*, 2010, **4**, 3147–3154.
2 S. U. M. Khan, M. Al-Shahry and W. B. Ingler, *Science*, 2002, **297**, 2243–2245.
3 A. Fujishima and K. Honda, *Nature*, 1972, **238**, 37–38.
4 L. Li, G. S. Rohrer and P. A. Salvador, *J. Am. Ceram. Soc.*, 2012, **95**, 1414–1420.
5 L. Li, P. A. Salvador and G. S. Rohrer, *Nanoscale*, 2014, **6**, 24–42.
6 L. Li, X. Liu, Y. L. Zhang, P. A. Salvador and G. S. Rohrer, *Int. J. Hydrogen Energy*, 2013, **38**, 6948–6959.
7 B. Oregan and M. Gratzel, *Nature*, 1991, **353**, 737–740.
8 G. Sauve, M. E. Cass, G. Coia, S. J. Doig, I. Lauermann, K. E. Pomykal and N. S. Lewis, *J. Phys. Chem. B*, 2000, **104**, 6821–6836.
9 G. W. P. Adhyaksa, G. I. Lee, S. W. Baek, J. Y. Lee and J. K. Kang, *Sci. Rep.*, 2013, **3**, 2711.
10 M. R. Hoffmann, S. T. Martin, W. Y. Choi and D. W. Bahnemann, *Chem. Rev.*, 1995, **95**, 69–96.
11 Y. Yao, G. Li, S. Ciston, R. M. Lueptow and K. A. Gray, *Environ. Sci. Technol.*, 2008, **42**, 4952–4957.
12 L. Li, Y. L. Zhang, A. M. Schultz, X. Liu, P. A. Salvador and G. S. Rohrer, *Catal. Sci. Technol.*, 2012, **2**, 1945–1952.
13 J. Du, X. Y. Lai, N. L. Yang, J. Zhai, D. Kisailus, F. B. Su, D. Wang and L. Jiang, *ACS Nano*, 2011, **5**, 590–596.
14 M. Ni, M. K. H. Leung, D. Y. C. Leung and K. Sumathy, *Renewable Sustainable Energy Rev.*, 2007, **11**, 401–425.
15 Q. Zheng, B. X. Zhou, J. Bai, L. H. Li, Z. J. Jin, J. L. Zhang, J. H. Li, Y. B. Liu, W. M. Cai and X. Y. Zhu, *Adv. Mater.*, 2008, **20**, 1044–1049.
16 P. Roy, S. Berger and P. Schmuki, *Angew. Chem., Int. Ed.*, 2011, **50**, 2904–2939.
17 W. J. Lee, J. M. Lee, S. T. Kochuveedu, T. H. Han, H. Y. Jeong, M. Park, J. M. Yun, J. Kwon, K. No, D. H. Kim and S. O. Kim, *ACS Nano*, 2012, **6**, 935–943.
18 A. Kongkanand, R. M. Dominguez and P. V. Kamat, *Nano Lett.*, 2007, **7**, 676–680.
19 D. L. Zhao, X. Yang, C. L. Chen and X. K. Wang, *J. Colloid Interface Sci.*, 2013, **398**, 234–239.
20 H. Zhang, X. J. Lv, Y. M. Li, Y. Wang and J. H. Li, *ACS Nano*, 2010, **4**, 380–386.
21 N. L. Yang, Y. Y. Liu, H. Wen, Z. Y. Tang, H. J. Zhao, Y. L. Li and D. Wang, *ACS Nano*, 2013, **7**, 1504–1512.
22 X. Y. Zhang, H. P. Li, X. L. Cui and Y. H. Lin, *J. Mater. Chem.*, 2010, **20**, 2801–2806.
23 G. W. Cui, W. L. Wang, M. Y. Ma, M. Zhang, X. Y. Xia, F. Y. Han, X. F. Shi, Y. Q. Zhao, Y. B. Dong and B. Tang, *Chem. Commun.*, 2013, **49**, 6415–6417.
24 D. K. Lee, K. S. Han, W. H. Shin, J. W. Lee, J. H. Choi, K. M. Choi, Y. Lee, H. I. Kim, W. Choi and J. K. Kang, *J. Mater. Chem. A*, 2013, **1**, 203–207.
25 Y. Cong, X. K. Li, Y. Qin, Z. J. Dong, G. M. Yuan, Z. W. Cui and X. J. Lai, *Appl. Catal., B*, 2011, **107**, 128–134.
26 R. Martel, T. Schmidt, H. R. Shea, T. Hertel and P. Avouris, *Appl. Phys. Lett.*, 1998, **73**, 2447–2449.
27 A. Kongkanand and P. V. Kamat, *ACS Nano*, 2007, **1**, 13–21.
28 K. Woan, G. Pyrgiotakis and W. Sigmund, *Adv. Mater.*, 2009, **21**, 2233–2239.
29 A. Peigney, C. Laurent, E. Flahaut, R. R. Bacsa and A. Rousset, *Carbon*, 2001, **39**, 507–514.
30 W. D. Wang, P. Serp, P. Kalck and J. L. Faria, *J. Mol. Catal. A: Chem.*, 2005, **235**, 194–199.
31 Y. Ou, J. D. Lin, S. M. Fang and D. W. Liao, *Chem. Phys. Lett.*, 2006, **429**, 199–203.
32 X. N. Dang, H. J. Yi, M. H. Ham, J. F. Qi, D. S. Yun, R. Ladewski, M. S. Strano, P. T. Hammond and A. M. Belcher, *Nat. Nanotechnol.*, 2011, **6**, 377–384.
33 G. Mamba, X. Y. Mbianda and A. K. Mishra, *Environ. Sci. Pollut. Res.*, 2014, **21**, 5597–5609.
34 W. Chen, Z. L. Fan, B. Zhang, G. J. Ma, K. Takanabe, X. X. Zhang and Z. P. Lai, *J. Am. Chem. Soc.*, 2011, **133**, 14896–14899.
35 V. R. Djokic, A. D. Marinkovic, O. Ersen, P. S. Uskokovic, R. D. Petrovic, V. L. R. Radmilovic and D. T. Janackovic, *Ceram. Int.*, 2014, **40**, 4009–4018.

36 W. Zhou, K. Pan, Y. Qu, F. F. Sun, C. G. Tian, Z. Y. Ren, G. H. Tian and H. G. Fu, *Chemosphere*, 2010, **81**, 555–561.
37 S. S. Kocha, D. Montgomery, M. W. Peterson and J. A. Turner, *Sol. Energy Mater. Sol. Cells*, 1998, **52**, 389–397.
38 C. Gomez-Navarro, R. T. Weitz, A. M. Bittner, M. Scolari, A. Mews, M. Burghard and K. Kern, *Nano Lett.*, 2007, **7**, 3499–3503.
39 L. D. Li, J. Q. Yan, T. Wang, Z. J. Zhao, J. Zhang, J. L. Gong and N. J. Guan, *Nat. Commun.*, 2015, **6**, 5881.
40 S. Sakthivel and H. Kisch, *Angew. Chem., Int. Ed.*, 2003, **42**, 4908–4911.
41 J. Tauc, R. Grigorov and A. Vancu, *Phys. Status Solidi*, 1966, **15**, 627–637.
42 L. B. Liao, Q. H. Zhang, Z. H. Su, Z. Z. Zhao, Y. N. Wang, Y. Li, X. X. Lu, D. G. Wei, G. Y. Feng, Q. K. Yu, X. J. Cai, J. M. Zhao, Z. F. Ren, H. Fang, F. Robles-Hernandez, S. Baldelli and J. Bao, *Nat. Nanotechnol.*, 2014, **9**, 69–73.
43 H. Mizoguchi, T. Kamiya, S. Matsuishi and H. Hosono, *Nat. Commun.*, 2011, **2**, 470.
44 H. Tang, K. Prasad, R. Sanjines, P. E. Schmid and F. Levy, *J. Appl. Phys.*, 1994, **75**, 2042–2047.
45 M. B. Bryning, D. E. Milkie, M. F. Islam, L. A. Hough, J. M. Kikkawa and A. G. Yodh, *Adv. Mater.*, 2007, **19**, 661–664.
46 L. A. Hough, M. F. Islam, P. A. Janmey and A. G. Yodh, *Phys. Rev. Lett.*, 2004, **93**, 168102.
47 K. H. Kim, Y. Oh and M. F. Islam, *Adv. Funct. Mater.*, 2013, **23**, 377–383.
48 S. Yoon, B. H. Ka, C. Lee, M. Park and S. M. Oh, *Electrochem. Solid-State Lett.*, 2009, **12**, A28–A32.
49 M. C. Long, Y. L. Qin, C. Chen, X. Y. Guo, B. H. Tan and W. M. Cai, *J. Phys. Chem. C*, 2013, **117**, 16734–16741.
50 M. A. Carreon, S. Y. Choi, M. Mamak, N. Chopra and G. A. Ozin, *J. Mater. Chem.*, 2007, **17**, 82–89.
51 K. H. Kim, M. Vural and M. F. Islam, *Adv. Mater.*, 2011, **23**, 2865–2869.
52 M. F. Islam, E. Rojas, D. M. Bergey, A. T. Johnson and A. G. Yodh, *Nano Lett.*, 2003, **3**, 269–273.
53 K. H. Kim, Y. Oh and M. F. Islam, *Nat. Nanotechnol.*, 2012, **7**, 562–566.
54 M. F. Islam, D. E. Milkie, C. L. Kane, A. G. Yodh and J. M. Kikkawa, *Phys. Rev. Lett.*, 2004, **93**, 037404.
55 L. A. Hough, M. F. Islam, B. Hammouda, A. G. Yodh and P. A. Heiney, *Nano Lett.*, 2006, **6**, 313–317.
56 S. Brunauer, P. H. Emmett and E. Teller, *J. Am. Chem. Soc.*, 1938, **60**, 309–319.
57 E. P. Barrett, L. G. Joyner and P. P. Halenda, *J. Am. Chem. Soc.*, 1951, **73**, 373–380.

Electronic Supplementary Material (ESI) for RSC Advances.

High Visible-Light Photochemical Activity of Titania Decorated on Single-Wall Carbon Nanotube Aerogels

Hang-Ah Park, Siyuan Liu, Paul A. Salvador, Gregory S. Rohrer and Mohammad F. Islam*

Department of Materials Science and Engineering, Carnegie Mellon University, 5000 Forbes Avenue, Pittsburgh, PA 15213, USA. E-mail: mohammad@cmu.edu

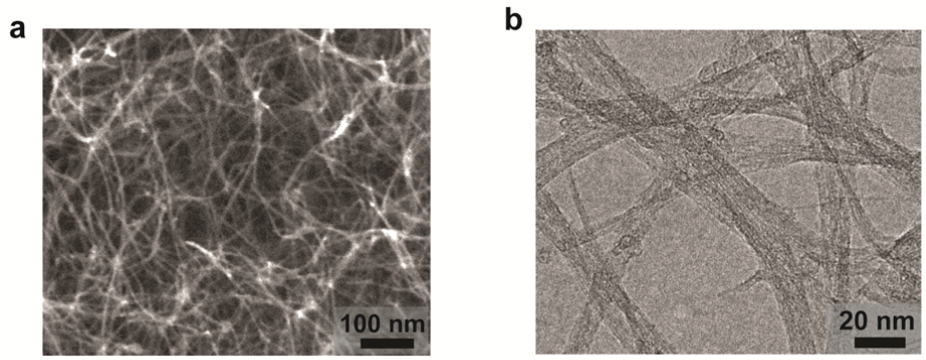

Fig. S1. a) High-resolution SEM and b) conventional TEM images of cross-sections of pristine single-wall carbon nanotube (SWCNT) aerogels.

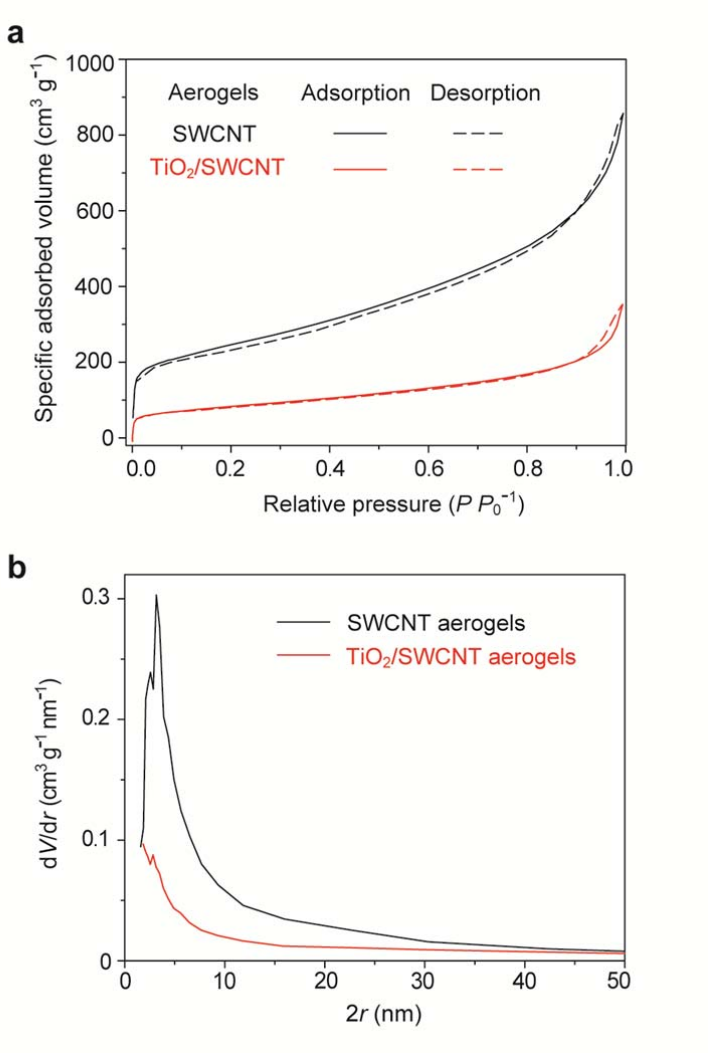

Fig. S2. a) Nitrogen adsorption–desorption isotherms of SWCNT and TiO_2/SWCNT aerogels with mass density of ≈ 9 mg mL^{-1} and ≈ 36 mg mL^{-1}, respectively. Specific adsorbed volume was calculated by dividing measured adsorbed volume by the mass of the sample and is plotted against the relative pressure, $P\ P_0^{-1}$, where P and P_0 are the equilibrium pressure and saturation pressure of nitrogen at the adsorption temperature of 77 K, respectively. b) Pore diameter distributions (dV/dr) of SWCNT aerogels and TiO_2/SWCNT aerogels as a function of pore diameter (2r). The pore characteristics within SWCNT aerogels can be tuned by changing the SWCNT concentration.[1]

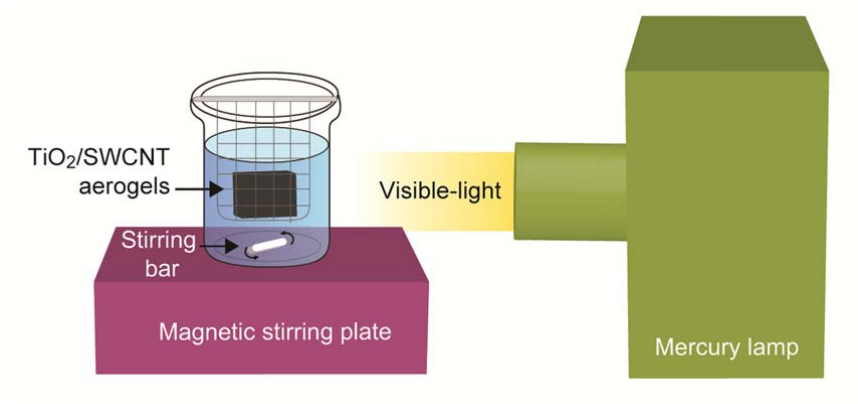

Fig. S3. Schematic illustration of photocatalytic dye degradation experimental setup.

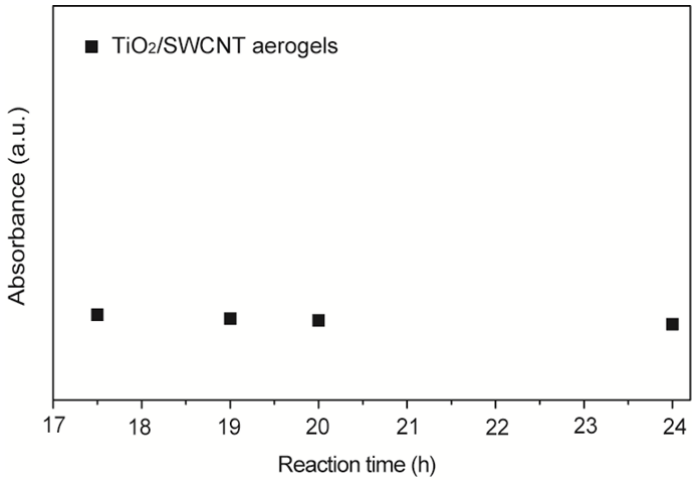

Fig. S4. Equilibration time for MB dye adsorption on TiO_2/SWCNT aerogels in the dark.

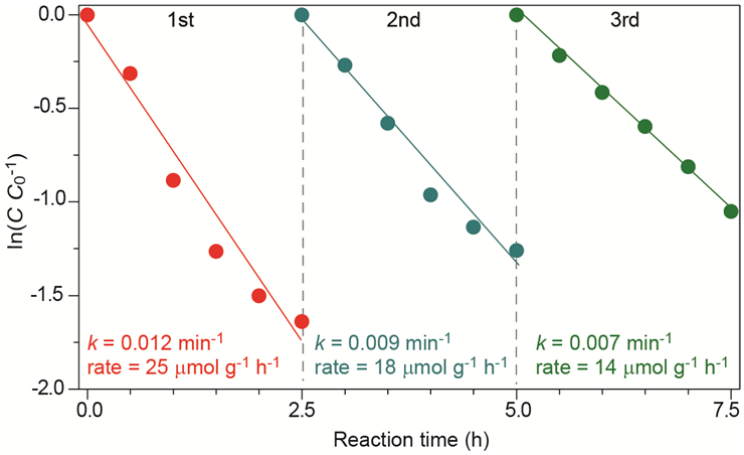

Fig. S5. Reusability of TiO_2/SWCNT aerogel composites for methylene blue dye degradation. The composites were rinsed in water after every 2.5 h of continuous use.

Table S1. Comparison of photocatalytic dye degradation performance by TiO_2 supported on carbon, graphene, or graphite.

Photocatalysts	Light source, power, spectral range	Adsorption-desorption equilibration time [h]	Dye:titania molar ratio[a]	Degradation rate[a] [μmol g^{-1} h^{-1}]	Rate constant[a] [min^{-1}]	Ref.
TiO_2/SWCNT aerogels	Hg, 300 W, visible	24	0.004	25 200[b]	0.012	This work
		24	0.032	25 (with fresh 0.02 mM dye solution)	0.0015	
TiO_2 P25/graphene	Xe, 500 W, visible	0.167	0.002	13.4	0.013	2
TiO_{2-x}/graphene	W, 500 W, visible	1	0.005	9.5	0.0045	3
TiO_2/graphene	Xe, 450 W, visible	1	0.0002	25[c]	0.034	4
TiO_2/graphene	Xe, 100 mW/cm^2, AM 1.5 solar simulator	0.5	0.003	13.7	0.019	5
TiO_2/carbon-dot	Xe, 1000 W, visible	Overnight	0.012	5.1	0.0047	6

[a] After dye adsorption to the samples had reached equilibrium in the dark.

[b] Estimated by taking the starting concentration of dyes before adsorption-desorption equilibration as C_0.

[c] Estimated by taking the starting concentration of dyes before adsorption-desorption equilibration as C_0 because the dye concentrations after equilibration are not provided. As such, the degradation rates and rate constants are likely to be significantly overestimated, particularly if supports had large surface area for dye adsorption.

References

1. K. H. Kim, Y. Oh and M. F. Islam, *Advanced Functional Materials*, 2013, **23**, 377-383.
2. H. Zhang, X. Lv, Y. Li, Y. Wang and J. Li, *ACS Nano*, 2010, **4**, 380-386.
3. M. Xing, X. Li and J. Zhang, *Scientific Reports,* 2014, **4**, 5493:1-7.
4. J. S. Lee, K. H. You and C. B. Park, *Advanced Materials*, 2012, **24**, 1084-1088.
5. M. Yang, Y. Liu, H. Wen, Z. Tang, H. Zhao,Y. Li and D. Wang, *ACS Nano*, 2013, **7**, 1504-1512.
6. G. Cui, W. Wang, M. Ma, M. Zhang, X. Xia, F. Hang, X. Shi, Y. Zhao, Y. Dong and B. Tang, *Chemical Communications,* 2013, **49**, 6415-6417.